Instantaneous Aqueous Spray Synthesis of Halide-Encapsulated $CsPb(Cl/Br)_3$ Quantum Dots for Stable Green to Pure-Blue Mini/Micro-LEDs

Ou Hai*, Xin An*, Peng Li, Weikang Dong, Keke Guan, Jiaxin Qin, Yuanting Wu

School of Materials Science and Engineering, Shaanxi Key Laboratory of Green Preparation and Functionalization for Inorganic Materials, Shaanxi University of Science and Technology, Xi'an, 710021, China

Corresponding author: Ou Hai
E-mail address: haiou@sust.edu.cn

Corresponding author: Xin An
E-mail address: 230212187@sust.edu.cn

Author: Peng Li
E-mail address: 230212133@sust.edu.cn

Author: Weikang Dong
E-mail address: 230212178@sust.edu.cn

Author: Keke Guan
E-mail address: 240211015@sust.edu.cn

Author: Jiaxin Qin
E-mail address: 240212132@sust.edu.cn

Author: Yuanting Wu
E-mail address: wuyuanting@sust.edu.cn

Table S1. Detailed parameters of samples 1-6

Sample	Reactant ratio	λ (nm)	FWHM (nm)	CIE (X, Y)
1	CsBr: $PbCl_2$: KCl=1:1:3	463	23	(0.1525,0.0941)
2	CsCl: $PbBr_2$: KCl=1:1:9	467	27	(0.1316,0.1459)
3	CsCl: $PbBr_2$: KCl=1:1:3	485	20	(0.0979,0.245)
4	CsCl: $PbCl_2$: KBr=1:1:3	501	20	(0.0716,0.5129)
5	CsCl: $PbBr_2$: KBr=1:1:3	508	24	(0.1116,0.6059)
6	CsBr: $PbBr_2$: KBr=1:1:3	520	27	(0.1561,0.6934)

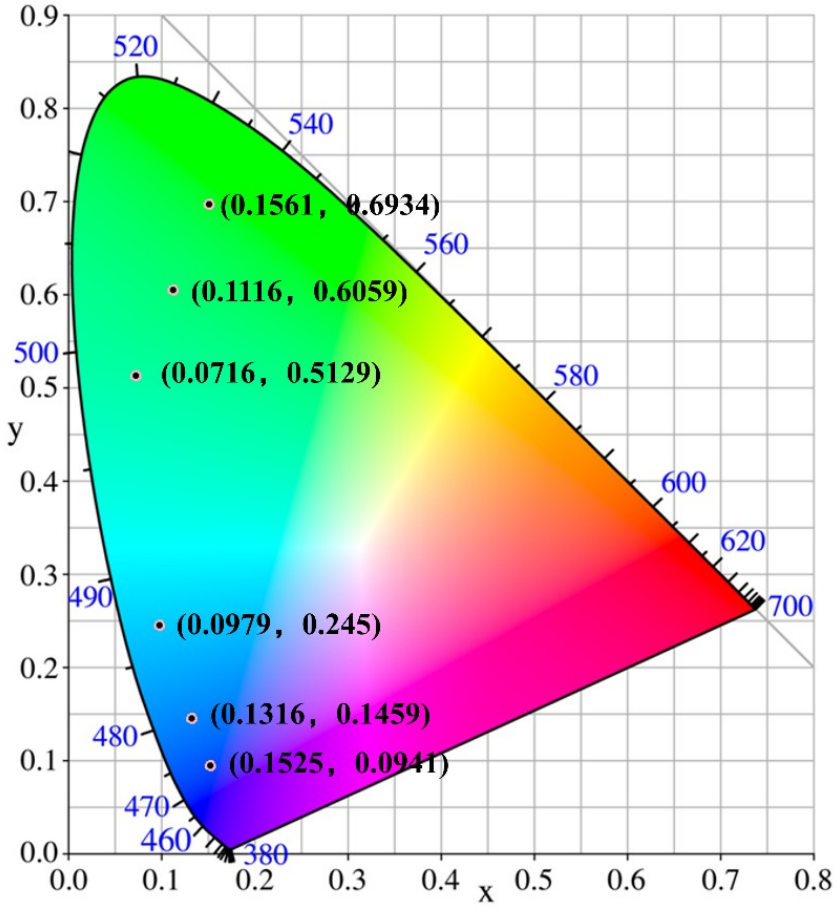

Figure. S1 CIE coordinate diagrams of samples 1-6

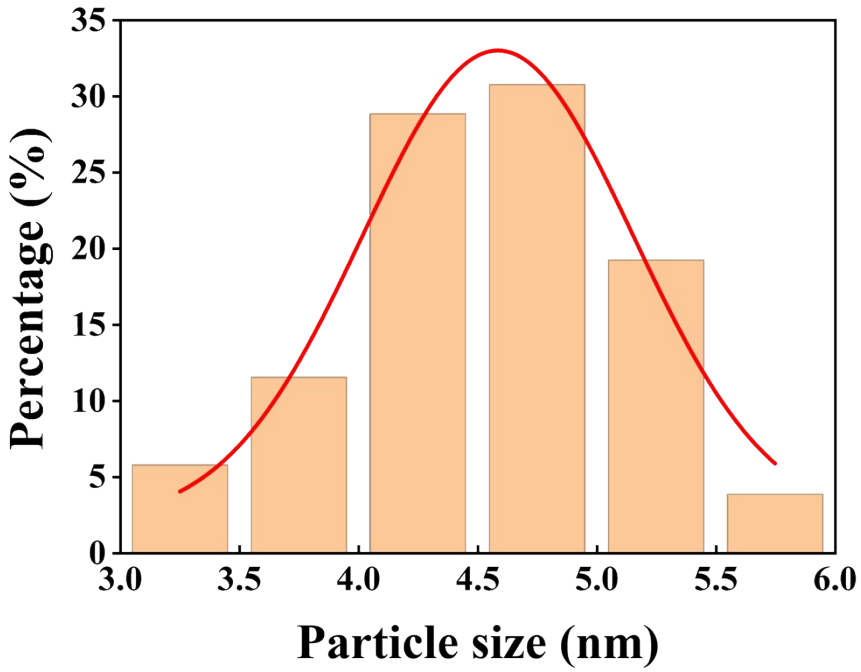

Figure. S2 Particle size distribution of $CsPb(Cl/Br)_3$ measured by spray drying method.

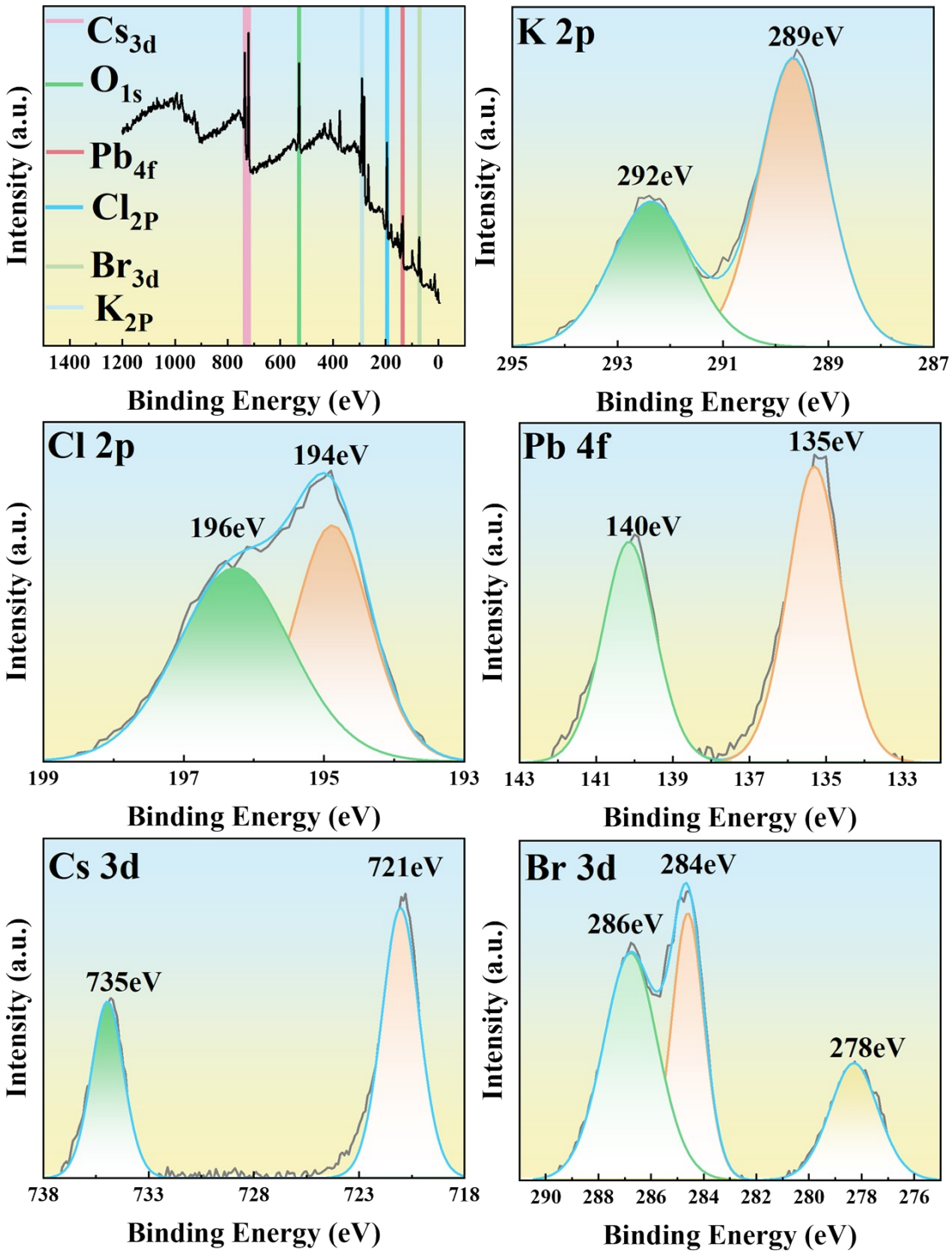

Figure. S3 High-resolution XPS spectra of Sample 1

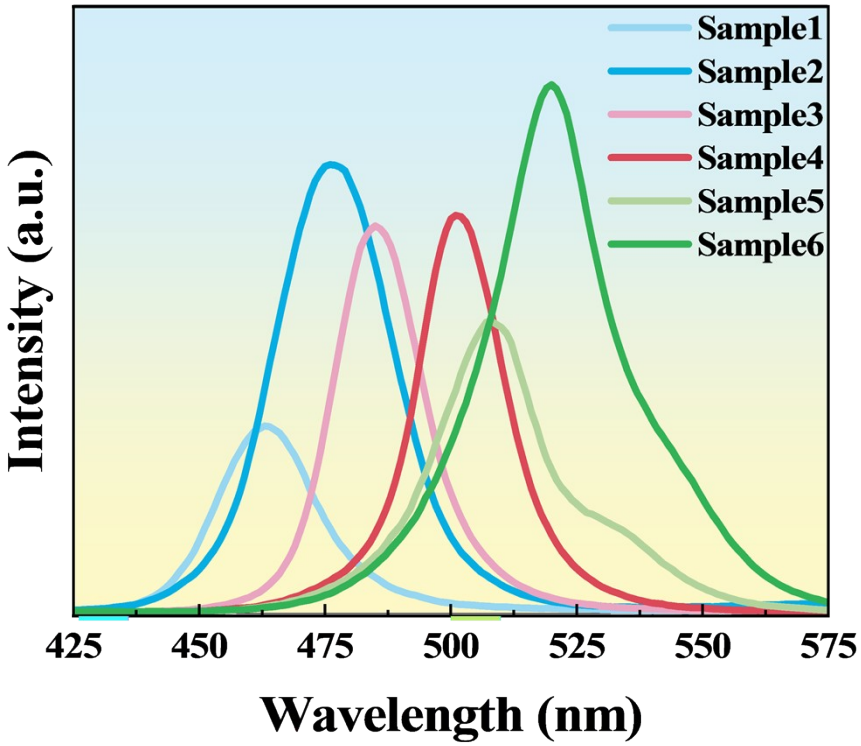

Figure. S4 The PL spectra of samples 1-6

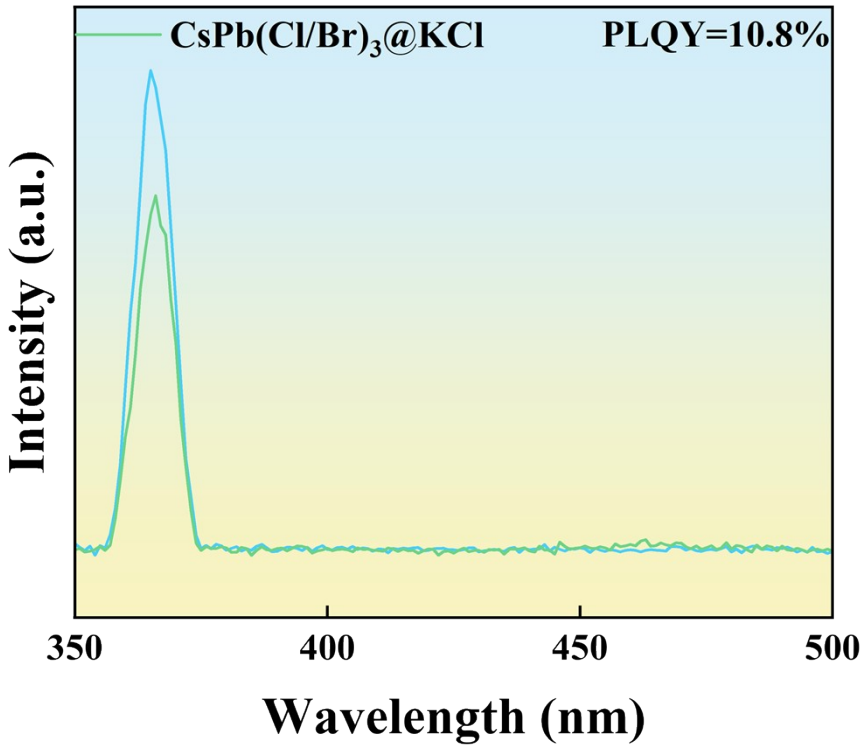

Figure. S5 The PLQY spectrum of $CsPb(Cl/Br)_3$@KCl

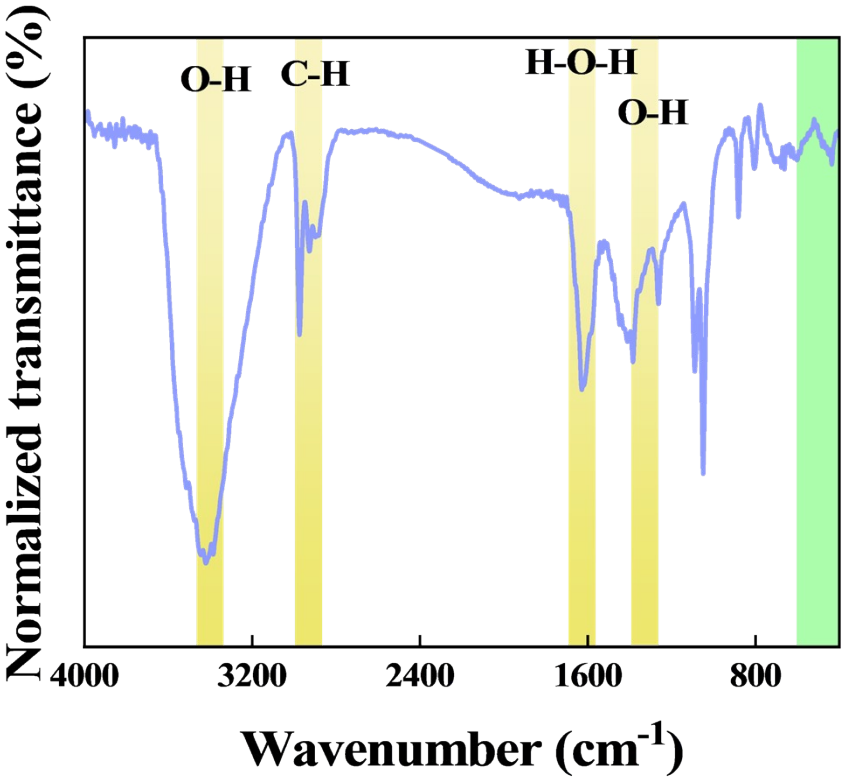

Figure. S6 FT-IR spectrum of Sample 1

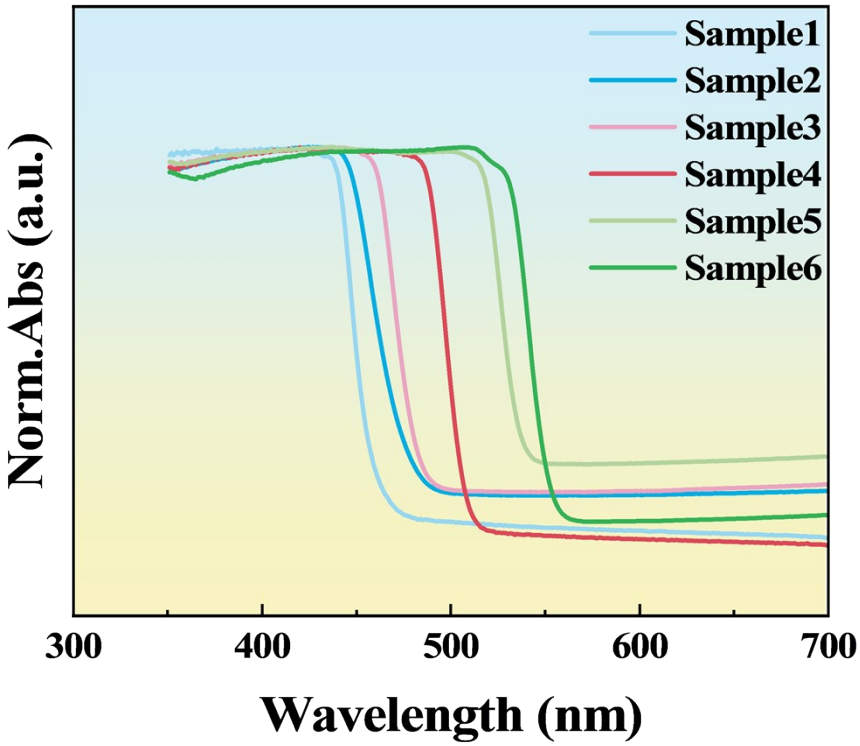

Figure. S7 Normalized absorption spectra of samples 1-6

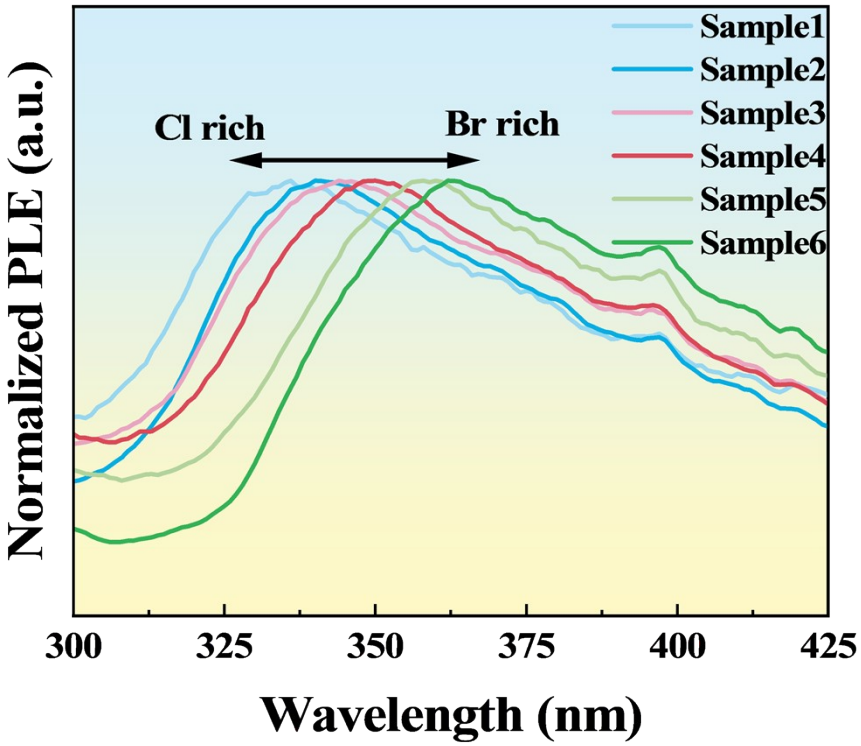

Figure. S8 Normalized PLE spectra of samples 1-6

Based on the determination of the three salts (CsBr: $PbCl_2$: KCl), we changed the amount of KCl to explore the influence of the variation in KCl content on the physicochemical properties of the prepared $CsPbCl_3$ nanoparticles, including: phase, excitation and emission intensity, peak position, and half-peak width.

With the increase of KCl content, the emission peak intensity of the samples shows an upward trend. When the KCl content reaches 7 mmol, the emission peak reaches its maximum value. The reason for this is that the excessive KCl provides a Cl-rich environment, which more effectively encapsulates the generated $CsPbCl_3$ perovskite quantum dots, protecting them from oxygen and external environmental damage, thereby enhancing their emission intensity.

In the XRD spectrum (Figure S9), we can observe the characteristic peaks of both the perovskite structure $CsPbBr_3$ and $CsPbCl_3$. Regardless of the sample proportion, there are peaks of both $CsPbX_3$ and KCl. The emission of the sample under a 365nm ultraviolet lamp appears as a deep blue color, and the emission peak is located at 463nm, indicating that $CsPbCl_3$ constitutes the majority in the sample. A deeper analysis of the XRD spectrum reveals that the peak at $2\theta = 31.9°$ is not a simple single peak but more resembles a double peak of the $CsPbCl_3$ PDF card, further demonstrating that the blue perovskite quantum dots can be successfully prepared by this method. The peak at $2\theta = 30.25°$ corresponds to the

characteristic peak of $CsPb_2Cl_5$ (PDF#97-024-9888), which decreases with the increase in KCl content, and disappears completely when the KCl content reaches 7mmol. This indicates that with the increase in KCl content, a transformation from $CsPb_2Cl_5$ to the $CsPbCl_3$ crystal form occurs (Equation S1). The peaks at 2θ = 22.4° and 31.9° correspond to the characteristic peaks of $CsPbCl_3$, which are respectively associated with the (101) and (200) crystal planes. The peaks at 2θ = 28.45° and 40.6° correspond to KCl, which are respectively associated with the (200) and (220) crystal planes. As shown in Figure S11, the emission intensity of the sample also increases and then decreases with the increase in KCl content, with a relatively narrow full width at half maximum (FWHM = 25nm). When the amount of KCl is 7mmol, the emission intensity of the sample reaches its maximum. In summary, through the analysis of XRD and PL spectra, we can conclude that only the phases of KCl and $CsPbCl_3$ exist in the perovskite powder material. And when n_{KCl} = 7mmol, the emission intensity of the material is at its optimal level, indicating that the perovskite powder material prepared by this method has high purity and emission intensity.

$$CsPb_2Cl_5 + CsCl \rightleftharpoons 2CsPbCl_3 \#(1)$$

In order to investigate the influence of drying temperature on the luminescence properties of perovskite powders, we carried out spray drying at different temperatures (90、100、110、120、130、140、

150℃). In this experiment, we selected four samples (90、110、130、150℃) from multiple temperature tests for analysis. As the temperature rises, it can be observed in the XRD spectra (Figure S12) that the broad peak at 2θ = 30.25° gradually disappears with the increase in temperature. However, in the PL spectra (Figure S14), it shows the best luminescence intensity at 110°C, indicating that at this temperature, the crystal form has been disrupted and transformed into the $CsPbCl_3$ perovskite phase. For the peaks of $CsPbCl_3$ and KCl, as the temperature increases, the peak intensity also increases, indicating that the higher the drying temperature, the higher the crystalline structure orderliness of each phase in the sample and the fewer defects in the crystal. However, the best luminescence intensity is only achieved at 110°C, and only at this temperature can KCl better interact with the $CsPbCl_3$ perovskite quantum dots to form a coating structure.

Subsequently, we changed the concentration of the prepared sample solution. We diluted the original perovskite solution from the highest concentration to the lowest concentration of 10, 8, 6, 4, and 2 mmol/L, and then carried out spray drying at 110℃. Analyzing its XRD (Figure S15) spectrum, we could observe that as the concentration of the perovskite solution increased, the intensity of the peak at 2θ = 30.25° gradually decreased, while the peak of $CsPbCl_3$ at 2θ = 39.4° gradually strengthened. This indicates that with the increase in the concentration of the perovskite solution, there is a certain crystal structure transformation during the

drying process at 110℃, from an unilluminating non-perovskite structure to the luminescent $CsPbCl_3$ perovskite structure. Therefore, in its PL (Figure S17) spectrum, we can see that the concentration of the perovskite solution has a significant impact on the luminescence intensity of the sample. As the concentration of the perovskite solution decreases, the emission peak intensity of the sample shows a decreasing trend.

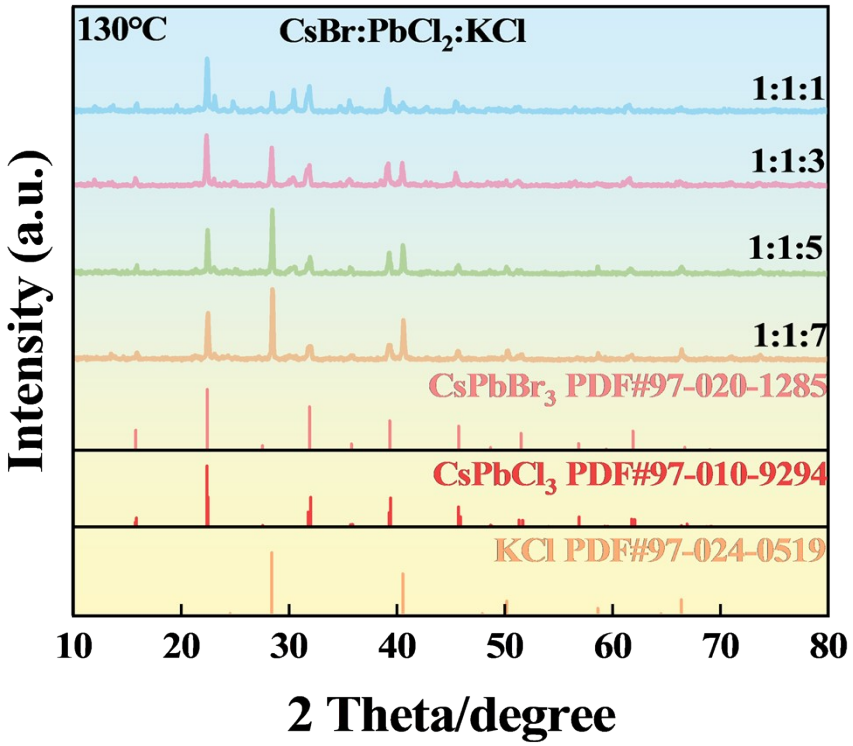

Figure. S9 The XRD spectrum of CsBr: $PbCl_2$: KCl = 1:1:X（X = 1、3、5、7）

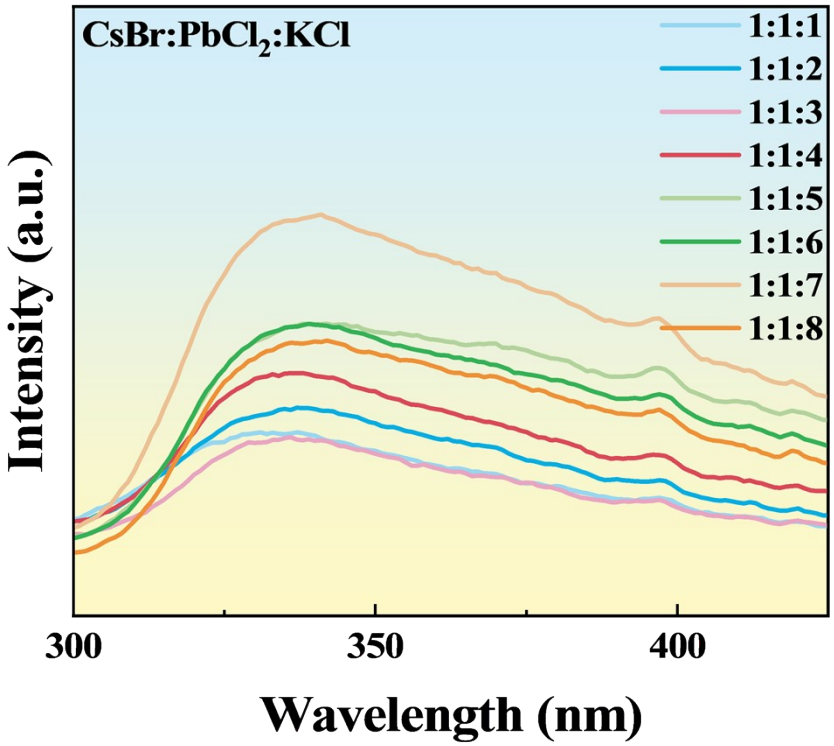

Figure. S10 The PLE spectrum of CsBr: $PbCl_2$: KCl = 1:1:X（X = 1-8）

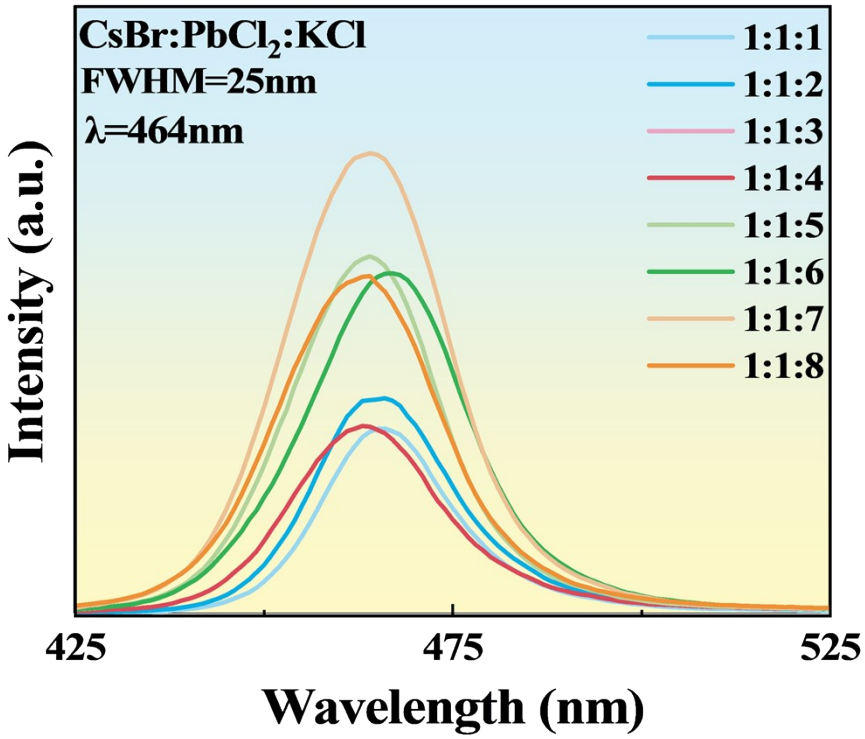

Figure. S11 The PL spectrum of CsBr: $PbCl_2$: KCl = 1:1:X（X = 1-8）

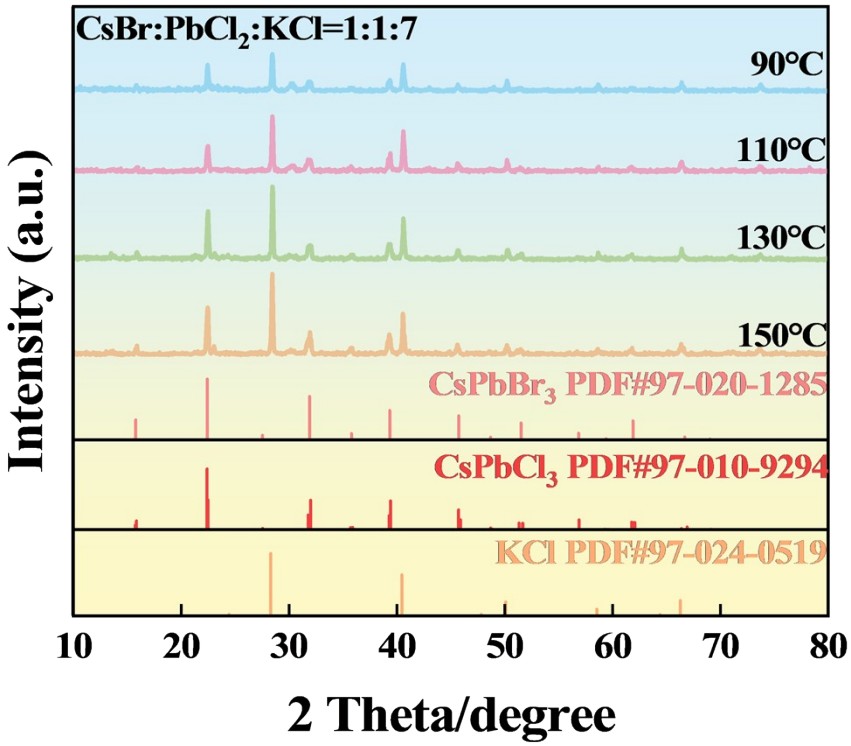

Figure. S12 The XRD spectra of sample CsBr: $PbCl_2$: KCl = 1:1:7 dried at different temperatures

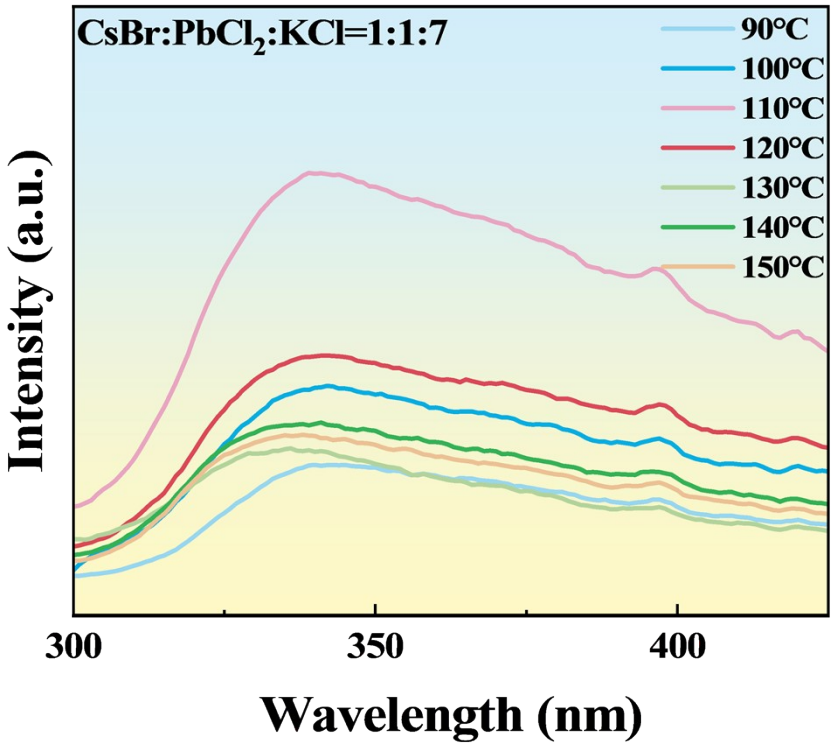

Figure. S13 The PLE spectra of sample CsBr: $PbCl_2$: KCl = 1:1:7 dried at different temperatures

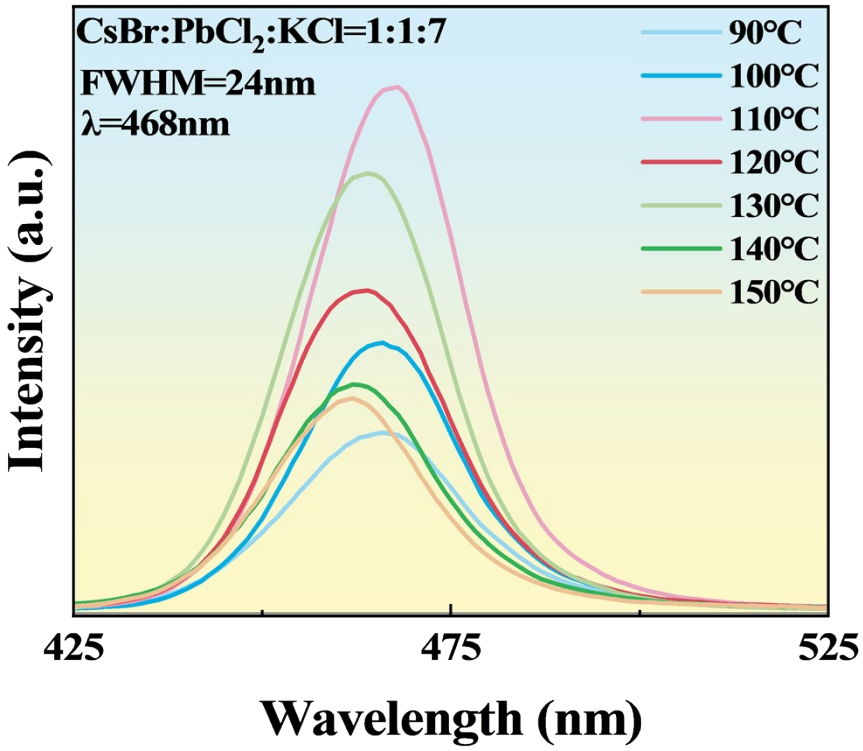

Figure. S14 The PL spectra of sample CsBr: $PbCl_2$: KCl = 1:1:7 dried at different temperatures

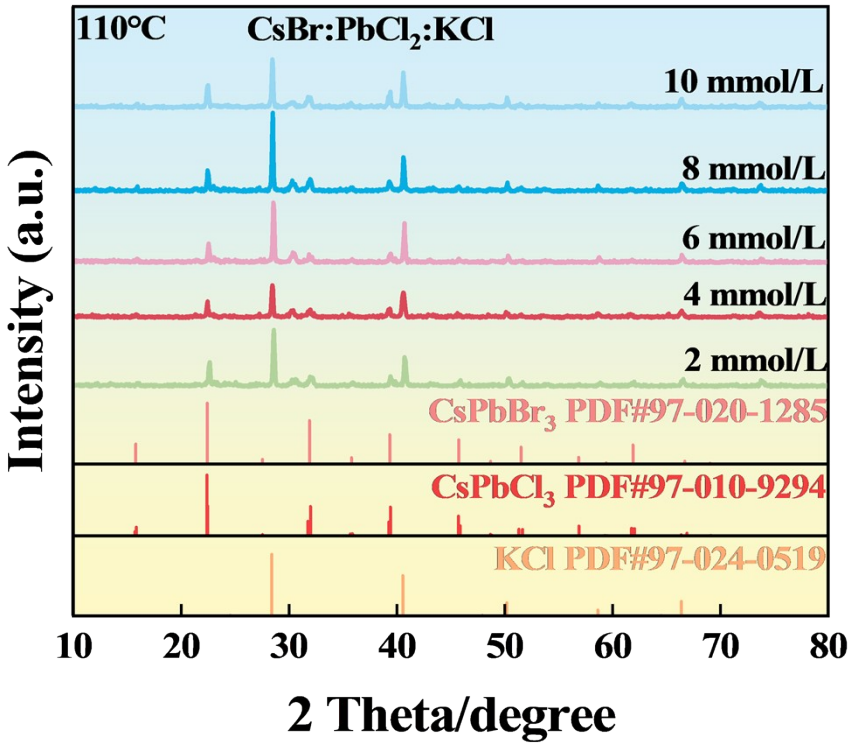

Figure. S15 XRD spectra of samples dried with perovskite precursor solutions of different concentrations at 110°C

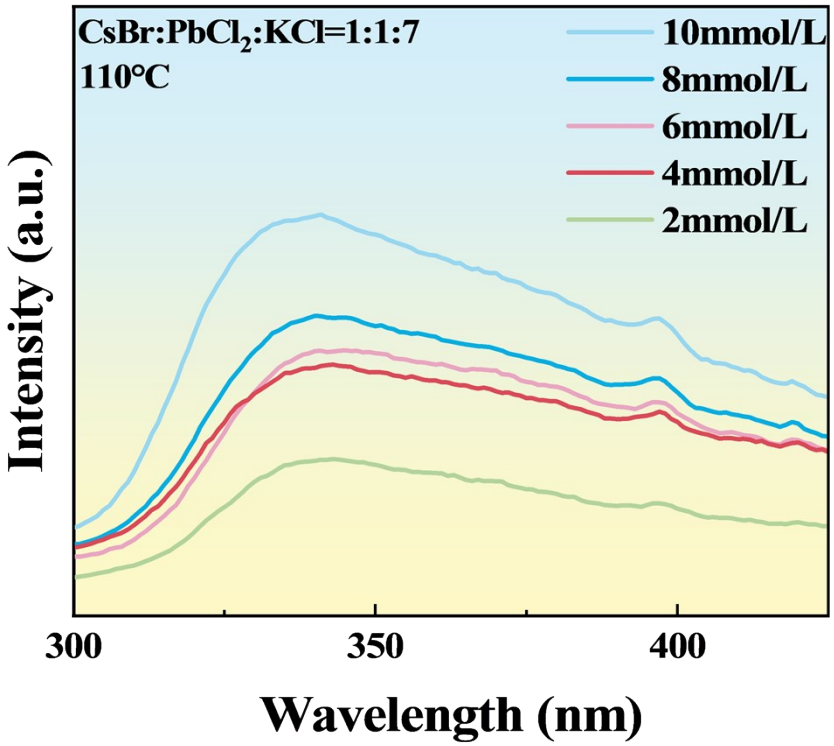

Figure. S16 PLE spectra of samples dried with perovskite precursor solutions of different concentrations at 110°C

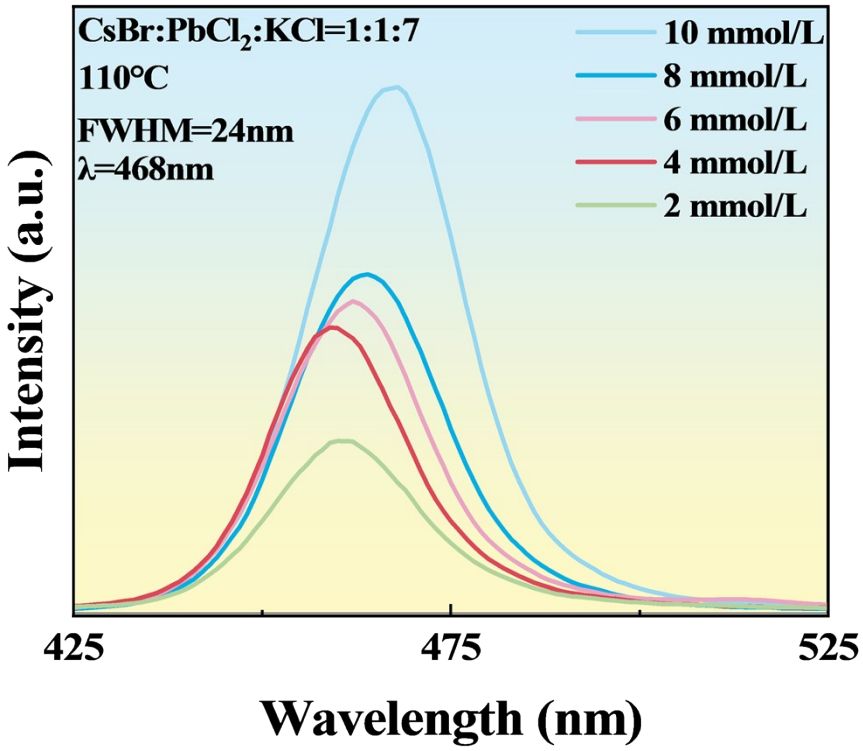

Figure. S17 PL spectra of samples dried with perovskite precursor solutions of different concentrations at 110°C

The time-resolved fluorescence spectra of the samples were tested and fitted using the double exponential function. The fitting equation is shown in Equation 2, and the formula for calculating the average lifetime is given in Equation 3.

$$I_t = I_0 + A_1\exp\left(-\frac{t}{\tau_1}\right) + A_2\exp\left(-\frac{t}{\tau_2}\right)\#(2)$$

$$\tau_{ave} = \frac{A_1\tau_1^2 + A_2\tau_2^2}{A_1\tau_1 + A_2\tau_2}\#(3)$$

T represents time, I_0 and I_t represent the initial and t-time emission intensities respectively, A_1 and A_2 are constants. The three attenuation times τ_1 and τ_2 respectively denote the two attenuation processes of their fluorescence radiation, and their attenuation lifetimes can be evaluated by their average lifetime τ_{ave}.

The fluorescence lifetime decay curves of samples 1-6 are shown in Figure S18. As can be seen in the figure, with the decrease in Cl ion content and the increase in Br ion content, the fluorescence lifetime of the samples shows a gradually decreasing trend. This is mainly attributed to the multiple effects brought about by the increase in Br content: Firstly, the substitution of Br for Cl leads to a reduction in the band gap of the material, while significantly increasing the effective mass of carriers, reducing the mobility, and making carriers more prone to being captured by defects; Secondly, the rich Br environment reduces the formation energy of

bromine vacancy deep-level trap defects, and exacerbates the lattice distortion caused by the size difference of halogen ions, resulting in a significant increase in the density of non-radiative recombination centers; Finally, the increase in Br content enhances the dielectric constant of the material, weakening the Coulomb binding force between electrons and holes, resulting in a decrease in the exciton binding energy, and making the free carriers after dissociation more prone to non-radiative recombination. These factors work together to significantly enhance the efficiency of the non-radiative recombination channel, thereby systematically shortening the overall fluorescence lifetime of the material.

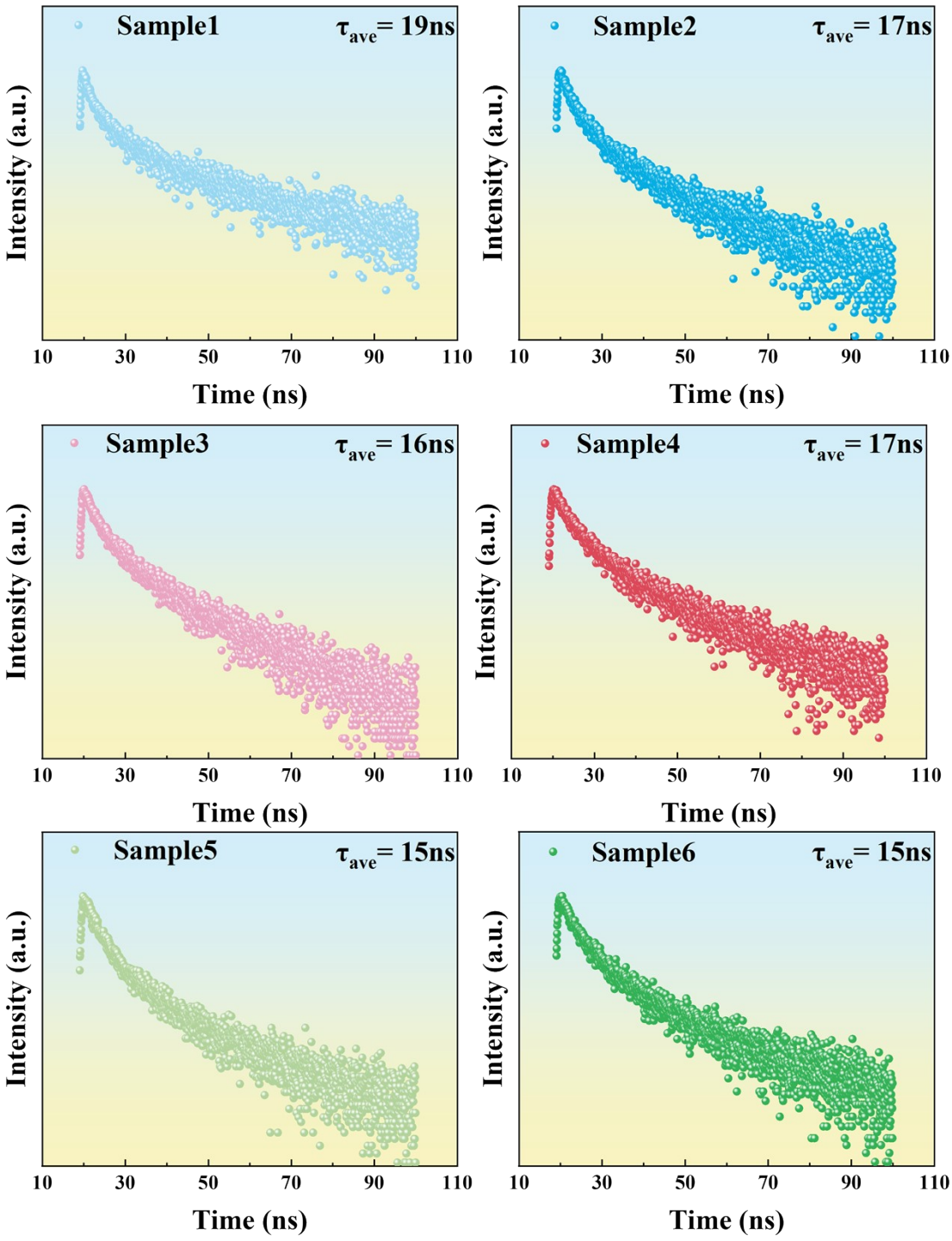

Figure. S18 PL decay curves of the sample1-6 fitted by bi-exponential model

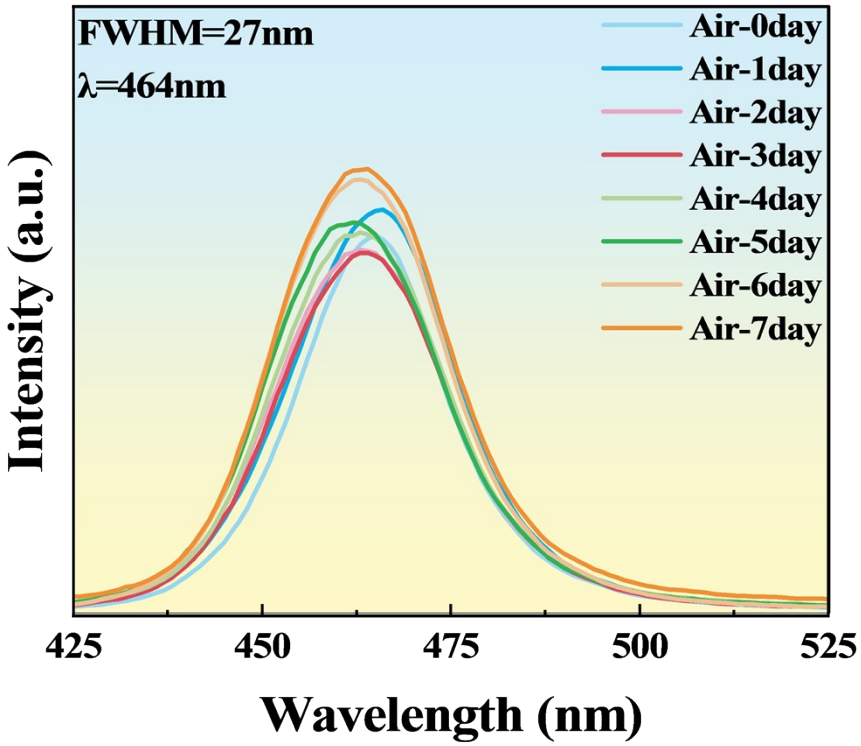

Figure. S19 The PL spectrum of sample1 exposed to the air for 7 days

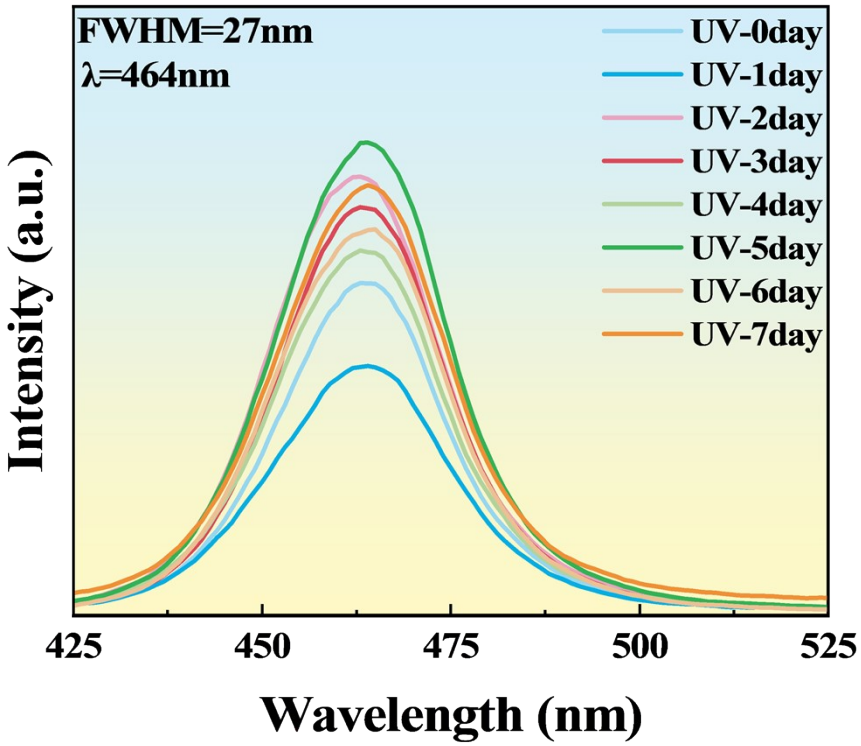

Figure. S20 The PL spectrum of sample1 exposed to the UV light (365 nm) for 7 days

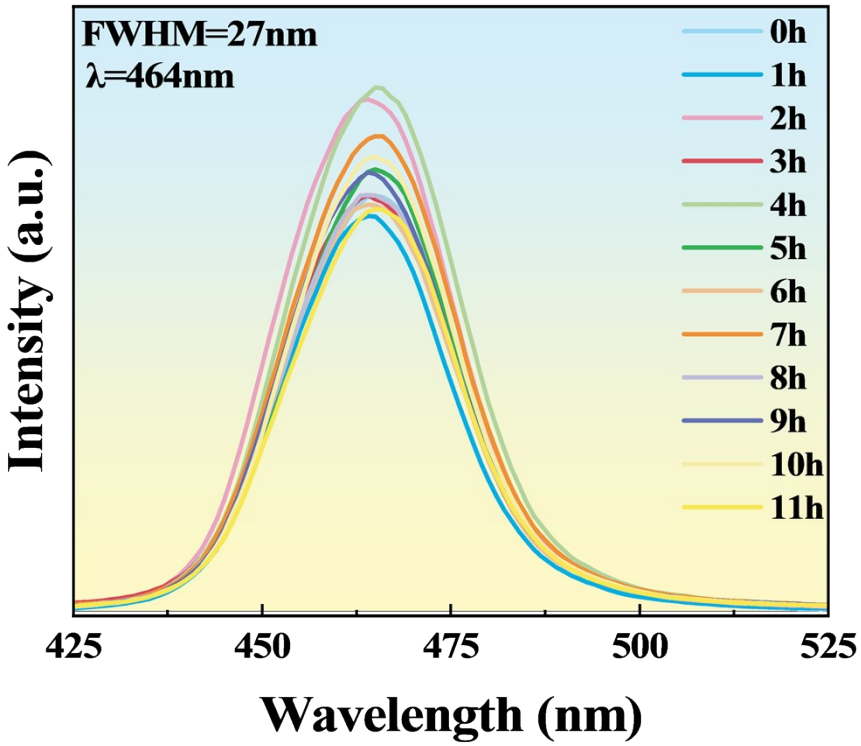

Figure. S21 The PL spectrum of sample1 exposed to the at 80℃ for 12 hours

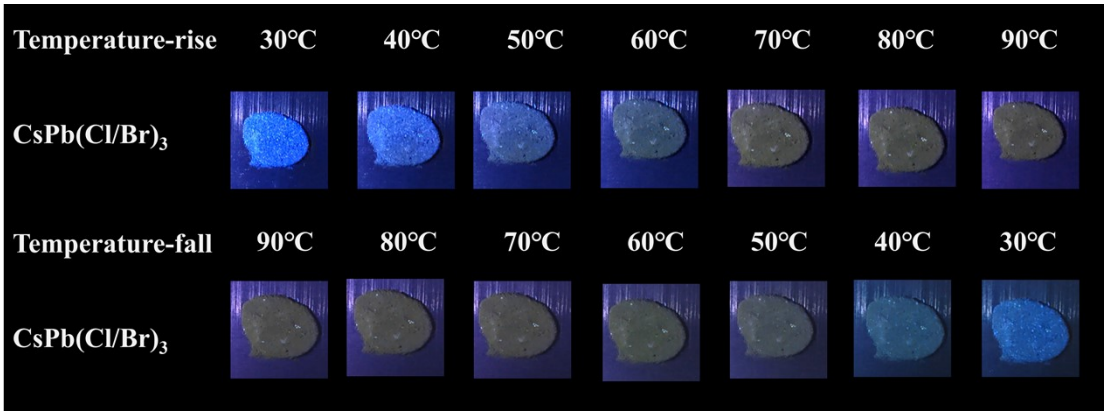

Figure. S22 Physical picture of Sample 1 being heated and cooled under a 365nm UV light

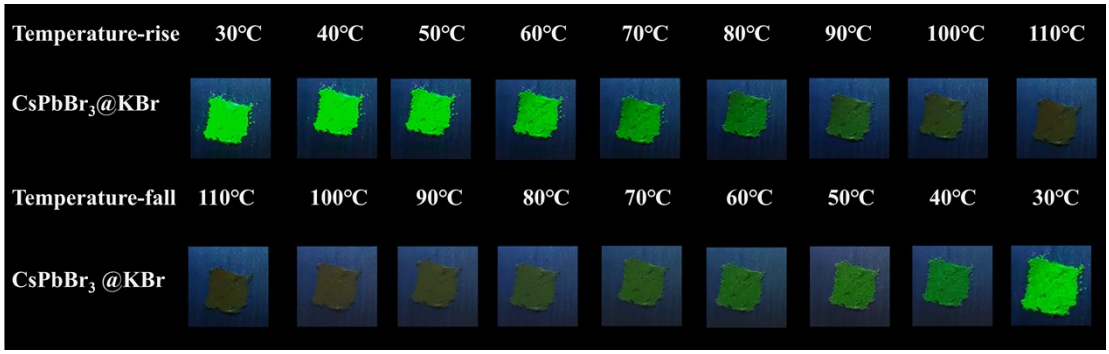

Figure. S23 Physical picture of Sample 6 being heated and cooled under a 365nm UV light

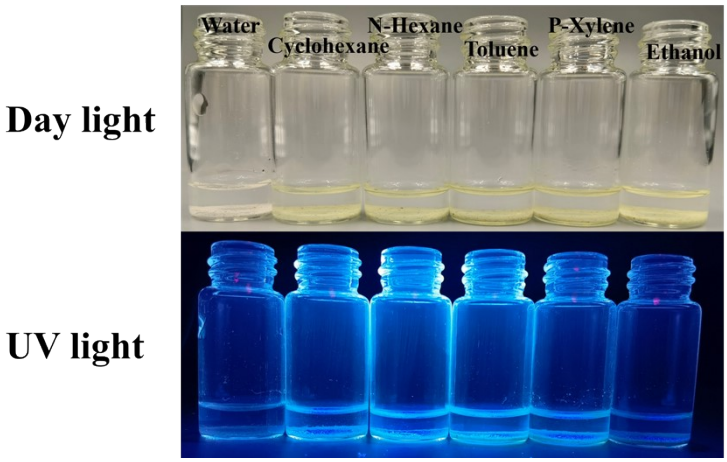

Figure. S24 Physical images of the luminescence of sample 1 under Day light and 365nm UV light in water and different organic reagents (from left to right: Water, Cyclohexane, N-Hexane, Toluene, P-Xylene, Ethanol)

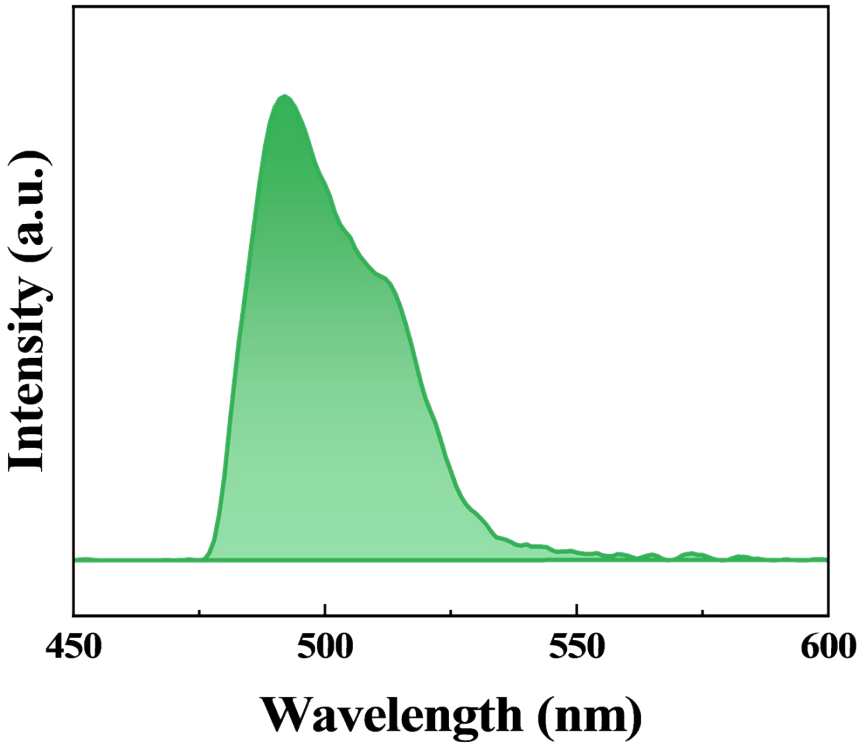

Figure. S25 The PL spectrum of the LED beads prepared by sample